



Lignin-derived Pt supported carbon (submicron)fiber electrocatalysts for alcohol electro-oxidation

F.J. García-Mateos^a, T. Cordero-Lanzac^a, R. Berenguer^a, E. Morallón^b, D. Cazorla-Amorós^c, J. Rodríguez-Mirasol^{a,*}, T. Cordero^a

^a Universidad de Málaga, Andalucía Tech, Departamento de Ingeniería Química, Campus de Teatinos s/n, 29010 Málaga, Spain

^b Departamento de Química Física e Instituto Universitario de Materiales, Universidad de Alicante, Apartado 99, E-03080 Alicante, Spain

^c Departamento de Química Inorgánica e Instituto Universitario de Materiales, Universidad de Alicante, Apartado 99, E-03080 Alicante, Spain

ARTICLE INFO

Article history:

Received 30 January 2017

Received in revised form 24 March 2017

Accepted 1 April 2017

Available online 3 April 2017

Keywords:

Binderless carbon electrode

Electrospun lignin fiber

Platinum

Phosphoric acid

Alcohol electro-oxidation

ABSTRACT

Lignin fibers, with and without phosphorus, and loaded with platinum have been prepared in a single step by electrospinning of lignin/ethanol/phosphoric acid/platinum acetylacetone precursor solutions. Thermochemical treatments have been carried out to obtain lignin-based carbon fiber electrocatalysts. The electrospun lignin fibers were thermostabilized in air and carbonized at 900 °C. The effect of phosphorus and platinum content on the porous texture, the surface chemistry and the oxidation/electro-oxidation resistance have been studied. Phosphorus-containing carbon fibers develop a higher surface area (c.a. 1200 m² g⁻¹), exhibit a lower Pt particle size (2.1 nm) and a better particle distribution than their counterpart without phosphorus (c.a. 750 m² g⁻¹ of surface area and 9.6 nm Pt particle size). It has been proved that phosphorus improves the oxidation and electro-oxidation resistance of the fibers, avoiding their oxidation during the preparation thermal stages and is responsible of the generation of a microporous material with an unusual wide operational potential window (1.9 V). An important Pt–P synergy has been observed in the oxygen transfer during the oxidation and electro-oxidation of the fibers. The obtained carbon fibers can act directly as electrodes without any binder or conductivity promoter. The fibers with platinum have shown outstanding catalyst performance in the electro-oxidation of methanol and ethanol.

© 2017 Elsevier B.V. All rights reserved.

1. Introduction

Fibers and composites have become one of the most studied materials due to their physical and chemical properties. Particularly, carbon fibrous materials have been widely studied because of the large spectrum of applications that they present [1]. Carbon fibers are usually obtained from polyacrylonitrile (PAN), pitch or rayon [2,3] and they exhibit outstanding mechanical properties [3]. On the other hand, renewable source of carbon, such as, lignin, has been proposed as carbon-fiber precursor as well [4,5]. Lignin is the second most abundant polymer in biomass after cellulose and it is the main co-product in the papermaking industry. However, the limited market of the lignin makes it an attractive raw material for “waste-refinery” or “bio-refinery” [6].

Lignin contains aromatic and phenolic groups that make it suitable as carbon precursor. Many applications have been proposed

to exploit its potential, in this way, lignin has been used to produce porous carbon materials of great interest in many applications as adsorbent [7,8], catalyst [9], or catalysts support [10]. Although Kraft lignin is more abundant than organosolv lignin, organosolv one is being more studied for these applications as natural carbon fiber source because of its low content in inorganic materials that makes it more environmentally friendly [11,12].

Carbonaceous materials, in many different conformations and structures (activated carbons, carbon black, carbon nanotubes, carbide-derived carbons, graphene sheets, etc.) have been studied in electrochemical applications [13–15]. On the other hand, platinum supported-carbon electrodes are receiving a growing interest because they are used as electrocatalysts in proton exchange membrane fuel cells (PEMFCs) and direct methanol fuel cells (DMFCs) [16–20]. The core part of these fuel cells is the preparation of the electrodes in which the platinum-based electrocatalysts are the most efficient.

Porous carbon materials have been considered as electrocatalyst supports for its properties. However, Pt supported carbon catalysts undergo from decreasing its performance during operation, being

* Corresponding author.

E-mail address: mirasol@uma.es (J. Rodríguez-Mirasol).

corrosion of the carbon supports one of the main reasons. The surface chemistry of carbon materials is important for their use as catalysts support and a key factor for improving their properties. In order to deposit metal catalysts on carbon materials uniformly and efficiently, surface chemistry modification is adopted as an effective method to change interfacial properties and improve the interaction between metal catalysts and carbon materials [21]. Then, the incorporation of N or P heteroatom surface groups is widely studied because these groups also enhance the electrochemical properties [22–24]. In particular, P-groups have been demonstrated to be an effective inhibitor of the carbon electro-oxidation, improving the electrocatalyst performance [24]. Nevertheless, the main drawback of commonly used powdered carbon supports is that a polymeric material must be added for binding the carbon grains and for obtaining a good current yield of carbon electrode. The binder (a non-conducting solid) could degrade the carbon electrode properties, and lead to the pore blockage and the decrease of the electrode conductivity.

Carbon fibers have many advantages over other carbon conformations, and show good flexibility, density, high surface area and, in some cases, excellent electrical conductivity [25]. In fact, as a continuous material, the conductivity of the fiber is much higher than that of particles obtained from the same precursor [13]. These properties make carbon fibers one of the best carbon conformations for electrochemical applications. Several promising results have been obtained with carbon fibrous materials as electrodes in interesting applications like energy storage [26], or solar cells [27]. Despite carbon fibers can be prepared by different ways, electrospinning method allows for easily obtaining a binderless carbon electrode from a precursor solution [13]. In addition to the good structural characteristics, it is possible to obtain a uniform dispersion of a metal all over the fibers by this method in a single step, yielding, after a thermal stabilization and carbonization, a final carbon fiber-based electrocatalyst with very well dispersed metallic particles of reduced diameter [28], which increases the metallic active surface of the catalyst.

In this work, a simple way for obtaining carbon fibers with relatively low content but very well distributed platinum nanoparticles to be used as electrocatalysts is presented. The conductivity of the lignin-based carbon fibers, prepared by co-electrospinning of lignin solution at room temperature without any additives apart from the platinum salt and phosphoric acid, enables the preparation of flexible electrode to work without any binder or conductivity promoter. The use of this kind of binderless electrodes with low platinum loading is a novel contribution from an application point of view. The porous texture, surface chemistry and oxidation/electrooxidation resistance of different carbon fibers catalysts (with and without platinum and phosphorus) has been analyzed. The obtained materials have been tested as electrocatalysts in methanol and ethanol electro-oxidation, paying attention to the above mentioned main advantages of these catalysts (i.e., low platinum loading, flexible electrodes and no binder is used), which are recognized as desirable properties of electrocatalysts for methanol and ethanol electrooxidation [29–33]. The use of low-Pt loading electrocatalyst for DMFCs and the obtaining of energy (via electro-oxidation) from ethanol, which can be obtained from lignocellulosic sources (bio-ethanol), are interesting strategies toward a more sustainable and efficient production of energy.

2. Experimental

2.1. Electrocatalyst preparation

Lignin fibers were prepared by electrospinning method using Alcell® lignin as precursor in a co-axial configuration [34] and

ethanol as solvent. The best electrospinning behavior was obtained when the weight ratio (lignin:ethanol) was 1:1. In the case of phosphorus-containing lignin fibers, the solution was prepared by mixing lignin:ethanol:H₃PO₄ (85%) with a weight impregnation ratio of 1:1:0.3 respectively. The solution was stirred over night at 200 rpm and 60 °C before spinning. In order to compare, lignin fibers and phosphorus-containing lignin fibers were prepared with different platinum concentrations to study the effect of metal. Different platinum acetylacetone concentrations were added to the initial solutions in order to obtain, in one step, lignin fibers and phosphorus-containing lignin fibers with platinum nanoparticles. The weight ratios (platinum acetylacetone:lignin) used, in both cases, to obtain a spinnable solution was 0.006:1 and 0.03:1 to prepare lignin fibers with low and high platinum concentrations (about 1 wt% and >5 wt% respectively). Platinum chloride is typically used as precursor to deposit platinum particles [35], however, the organic salt shows advantages against the inorganic. Acetylacetone anion can add some carbon chain to the support in the thermal treatment, and acetone evaporation can improve the porous texture of the fiber due to its size.

In the electrospinning system, a typical Taylor cone is formed in the needle due to the electrical field generated between the tip and the collector [28,34]. For lignin fibers, the applied electrical potential difference was 14 kV (the collector was at -7 kV and the tips at +7 kV), however, phosphorus-lignin fibers need an electrical voltage of 22 kV (collector at -11 kV and tip at +11 kV) to form the Taylor cone due to the electrostatic interactions caused by the phosphoric acid. Ethanol was pumped through the external needle as solvent to avoid the solidification of the cone. The ethanol and lignin solution flow rates were 0.1 and 1 mL h⁻¹, respectively, for the preparation of lignin fibers. In case of the initial lignin solution containing phosphoric acid, the flow rates needed were 0.3 mL h⁻¹ for ethanol and 3 mL h⁻¹ for lignin/H₃PO₄ solution. The tip-to-collector distance was 25 cm.

Lignin fibers were thermostabilized in air from room temperature up to 200 °C with a heating rate of 0.08 °C min⁻¹ followed by 100 h of isothermal treatment in a tubular furnace with an air flow of 50 cm³ STP min⁻¹, whereas for phosphorus-containing fibers the thermostabilization temperature (also 200 °C) was reached at 0.8 °C min⁻¹, and maintained for 1 h. Stabilized fibers were carbonized in the same tubular furnace up to 900 °C, with a continuous flow of N₂ (150 cm³ STP min⁻¹) and a heating rate of 10 °C min⁻¹, in order to obtain lignin-based carbon fibers with and without phosphorus (PCFs and CFs, respectively) and with different platinum concentrations: with no platinum (PCF and CF), with low platinum concentration (PCFLPt and CFLPt) and with high platinum concentration (PCFH₃PO₄ and CFH₃PO₄). Phosphorus-containing lignin-based carbon fibers (PCFs) were washed with distilled water at 60 °C to neutral (or constant) pH and negative phosphate analysis in the eluate to remove the remaining phosphoric acid after the carbonization stage.

2.2. Characterization

The porous texture was characterized by N₂ adsorption-desorption at -196 °C and by CO₂ adsorption at 0 °C, using a Micromeritics ASAP2020 apparatus. Samples were previously outgassed for 8 h at 150 °C under vacuum. From the N₂ adsorption/desorption isotherm, the specific surface area (A_{BET}) was calculated using the BET equation. The micropore volume (V_t) and the external surface area (A_t) were determined using the t-method. The mesopore volume (V_{mes}) was calculated as the difference between total pore volume (at relative pressure of 0.995) and micropore volume [36]. Finally, the narrow micropore volume (V_{DR}) and the narrow micropore surface area (A_{DR}) were estimated by applying the Dubinin–Radushkevich equation to the

CO_2 adsorption isotherm [37]. Pore size distribution was determined from N_2 adsorption isotherm by 2D-NLDFT heterogeneous surface model [38].

The surface chemistry of CFs and PCFs was studied by X-ray photoelectron spectroscopy (XPS), the analyses were carried out in a 5700 C model Physical Electronics apparatus with $\text{MgK}\alpha$ radiation (1253.6 eV). The C1s peak position was located at 284.5 eV [9] and used as reference to locate the other peaks, and the fitting of the XPS peaks was done by least squares using Gaussian–Lorentzian peak shapes.

The oxygen surface groups were also analyzed by temperature-programmed desorption (TPD). TPD experiments were carried out in a customized quartz fixed-bed reactor placed inside an electrical furnace and coupled to a non-dispersive infrared (NDIR) gas analyzer Siemens ULTRAMAT 22. A carbon fiber sample of 100 mg was heated from room temperature to 930 °C at a heating rate of 10 °C min⁻¹ in a 200 cm³ (STP)/min N_2 (99.999%) flow.

Scanning electron microscopy (SEM), using a JSM 6490LV JEOL microscope working at 25 kV, and transmission electron microscopy (TEM), in a Phillips CM200 microscope at an accelerating voltage of 200 kV, were used to study the fibers morphology. Platinum particle sizes were estimated with an image analyzer software.

The oxidation of the carbon fibers was evaluated by thermogravimetric (TG) analysis in a CI Electronics MK2 balance under 150 cm³ (STP) min⁻¹ air flow from room temperature up to 900 °C with a heating rate of 10 °C min⁻¹ using about 10 mg of carbon fiber.

2.3. Electrochemical characterization

The electrochemical characterization was carried out in a standard three electrode cell using a Pt wire as counter electrode and an Ag/AgCl/KCl 3 M electrode as the reference one. The working electrode was prepared by contacting a round piece (ca. 0.1 mg) of the carbon fibers with the tip of a glassy carbon rod (3 mm diameter), used as current collector. Thus, the nominal Pt loading in the tested electrodes is as low as 0.014 and 0.071 mgPt cm⁻² (for the CFs with lower and higher Pt content, respectively). The electric contact between the CFs and the collector was better attained by using a drop of Nafion solution (5 wt% Nafion® perfluorinated resin solution, Aldrich). Therefore, neither any binder nor any conductivity promoter were used for the utilization of the carbon fibers as electrodes. A 0.5 M H_2SO_4 aqueous solution was used as supporting electrolyte. N_2 (99.999%) was bubbled in the cell before the analysis to eliminate dissolved oxygen in the electrolyte.

The electrochemical properties of the fibers were studied by cyclic voltammetry, with a scan rate of 10 mV s⁻¹. Particularly, in order to study the electrochemical stability of the different CFs, the electrode potential was stepwise shifted by 0.1 V: (i) firstly, from the open circuit potential (OCP) to negative values until the observation of the hydrogen evolution reaction (HER). The onset potential for the HER was indicative of the lower limit potential (LLP) of the electrodes; and (ii) secondly, from the LLP to positive potentials above the OCP, until the observation of anodic currents accompanied with an increase in the intensity of faradic processes in the subsequent cycles. Since these processes are inherent to electro-active oxygen surface groups, both facts occurring together are considered an evidence of carbon electro-oxidation. The onset potential of these anodic currents were then indicative of the upper limit potential (ULP) of the electrodes.

The different lignin-based carbon fiber electrodes were tested as electrocatalysts for the methanol and ethanol oxidation reactions (MOR and EOR, respectively). The experiments were carried out in a similar three electrode cell under the presence of 1.5 M alcohol solution. To ensure reproducibility, the electrodes were first electrochemically stabilized by cyclic voltammetry in the absence of

Table 1
Stabilization and carbonization yields.

Sample	Stabilization yield (wt%)	Carbonization yield (wt%)	Overall yield (wt%)
CF	73.2	36.9	27.0
CFLPt	62.8	37.2	23.4
CFHPt	44.5	22.3	9.9
PCF	88.2	32.9	29.0
PCFLPt	87.5	33.4	29.2
PCFHPt	85.1	35.0	29.8

alcohols under an operational potential window of –0.2 to 0.9 V or –0.2 to 1.2 V (vs. Ag/AgCl/KCl 3 M), for CFs or PCFs, respectively. Next, the electrode was immersed at 0.0 V (controlled potential) in a second cell containing the supporting electrolyte and 1.5 M alcohol solution. After current stabilization, the electrode potential was scanned at 10 mV s⁻¹ up to 0.9 V (or 1.2 V in the case of PCFs) and repeatedly cycled between –0.2 and 0.9 V (or 1.2 V) until a stable voltammogram was achieved (the reported steady voltammograms were usually registered at the 10th cycle).

After the voltammetric characterization some electrodes were subsequently submitted to chronoamperometric measurements at different potentials. Different electrode potential was increased from 0.0 V to 0.5, 0.6 or 0.7 V. All the electrochemical measurements experiments were performed using a Biologic VSP 300 potentiostat.

3. Result and discussion

3.1. Carbon electrocatalyst preparation

Table 1 reports the stabilization and carbonization yields of the different carbon fibers prepared in this work. During the stabilization stage, the polymeric lignin chains suffer cross-linking reaction and the fibers surface takes oxygen producing carbonyl, carboxyl, anhydride and ester surface groups [34,39]. Some oxygen groups can leave the structure as evolved CO and CO_2 . Surface phosphorus groups are more capable of taking oxygen, forming different surface carbon–oxygen–phosphorus complexes (mainly C–O–PO₃ and C–PO₃) [40]. In the carbonization stage up to 900 °C, volatile carbon compounds leave the solid and oxidation reactions take place with the retained oxygen during the stabilization process [28], forming complex and condensed carbon structures in the final product. Phosphoric acid acts as activating agent, anchoring on the fibers surface different phosphorus groups and generating a developed porous texture in the final carbon fibers.

Lignin-based carbon fibers (CFs) and phosphorus-containing lignin-based carbon fibers (PCFs) preparation present different yields (**Table 1**). Likewise, these materials show different behavior during the stabilization and carbonization steps when platinum is present in their composition. The stabilization yields of CFs are lower than those of PCFs, which should be attributed to the effect of P. In the presence of Pt, the stabilization yields of CFs decrease, and the higher the amount of metal in the lignin fibers, the lower the yield is observed. This could be related to the high activity of a well-known oxidation catalyst like Pt [41]. However, independently of the Pt content, the PCFs show similar stabilization yields as can be observed in **Table 1**. This result indicates that phosphorus prevents the oxidation of the fibers surface during the stabilization stage, even in the presence of platinum.

In addition, the presence of phosphorus–carbon groups allows a 10–60 times faster stabilization process. As lignin presents a glass transition temperature (T_g) far below the carbonization temperature, as-spun fibers need to be stabilized to avoid softening and fibers melting. Air oxidation is an easy and cheap process of stabilization [28,39] due to the increase of the T_g through oxygen cross-linking reactions and oxygen groups formation. Slow heating

rates are needed in the air stabilization process to ensure a temperature lower than the T_g . The presence of H_3PO_4 in the as-spun fibers increases the amount of oxygen surface content. Therefore, the cross-linking reactions and the formation of oxygen groups (with and without Pt) are favored in this case. This way, the stabilization of P-containing lignin fibers can be carried out at faster heating rate and less time without fibers melting in the carbonization step.

When stabilized fibers were heat-treated up to 900 °C in N_2 atmosphere, the carbonization yields (referred to the stabilized fibers) are similar for all the experiments (about 35%), except for CFHPT (Table 1). This low carbonization yield corresponds to the lowest stabilization yield obtained in the first thermal treatment. Hence, it is possible to conclude that CFHPT takes a huge amount of oxygen in the stabilization stage (due to the high percentage of metal in its surface), which is partially removed during the carbonization stage as CO_2 and CO .

Comparison of the overall yields (loss of oxidation products and volatile carbon compounds) of the fibers (Table 1) indicates that CF and PCF present similar yields (about 30 wt%). However, the presence of Pt in CFs produces a very different behavior as said above: the high oxygen content of the fibers after stabilization treatment in CFLPT and CFHPT, and the absence of an oxidation inhibitor (as phosphorus) favor carbon gasification during the subsequent carbonization process, producing a development of mesoporosity as will be discussed in the next section. On the contrary, the presence of P inhibits the carbon oxidation even in the presence of Pt, thus, quite similar and higher overall yields are obtained for the production of Pt supported carbon fibers (PCFLPT and PCFHPT).

3.2. Physicochemical characterization

Fig. 1 shows the N_2 adsorption–desorption isotherms at –196 °C for the different carbon fibers with or without phosphorus and with or without platinum. Textural parameters derived from these isotherms are displayed in Table 2. CFs exhibit between 750 and 850 $m^2 g^{-1}$ BET surface area, while PCFs can develop more than 1100 $m^2 g^{-1}$ BET surface area. These results indicate that H_3PO_4 produces an additional development of porosity in phosphorus-containing fibers. However, these fibers do not develop wide mesopores as the impregnation ratio used for the chemical activation ($g H_3PO_4/g$ precursor) is lower than 1 (0.3 in this case) [9,42]. This different behavior can also be appreciated by comparing the isotherms of CF and PCF (Fig. 1a and c), which show that PCF is able to adsorb more nitrogen at lower relative pressures than the phosphorus-free counterpart (CF).

The effect of platinum on the porous texture of CFs is shown in Fig. 1a. While CF exhibits a type I isotherm (characteristic of microporous materials), CFLPT and CFHPT present a type IV isotherm, with a hysteresis loop beyond 0.4 relative pressures, typical of materials with wide mesopores. In the absence of P, platinum produces a development of mesoporosity in the carbon fibers, being more appreciable as Pt content increases. This result may be attributed to the aforementioned high oxygen content after the fiber stabilization [34] and the Pt-promoted gasification of some carbon material during the thermal processes, which reduces the overall yield (Table 1). Pore size distribution (Fig. 1b) shows a reduction of the microporosity, shifting the maximum of the micropore size distribution to slightly higher values upon increasing the amount of Pt in CFs. Moreover, CFLPT and CFHPT develop new pores bigger than 20 Å as result of the greater surface oxidation of these carbon fibers.

By contrast, PCFs show type I isotherms (Fig. 1c), typical of microporous solids (this type of isotherm are usually obtained with a low amount of phosphoric acid [42]). This result evidences that Pt does not induce the mesoporosity generation in PCFs although they withhold more oxygen in the stabilization process than CFs. PCF and

PCFLPT present practically overlapped isotherms, which suggests the total inhibition of the Pt-catalyzed gasification reaction. However, the increase in BET surface area in PCFHPT indicates that this higher amount of platinum allows some gasification, developing higher pore volume on the carbon surface (Table 2). Fig. 1d displays the pore size distribution of these P-containing carbon fibers. A smaller micropore size is shown by carbon fibers with platinum, which means that in this case the oxidation of the carbon surface generates narrower microporosity.

As it is possible to observe in Table 2, CFs show a more pronounced increase in external surface area and mesopore volume than PCFs upon increasing the amount of platinum. This suggests that the presence of phosphorus plays a key role in the porosity development of the fibers during the thermal stages. Comparing the parameters obtained from CO_2 isotherms (Table 2), PCFs exhibit values of narrow micropore area (A_{DR}) and narrow micropore volume (V_{DR}) quite similar to the results obtained from N_2 isotherms (A_{BET} and V_t). On the other hand, for CFs, only CF presents higher narrow micropore area and volume calculated from CO_2 isotherm than BET surface area and micropore volume (V_t) determined from N_2 isotherm, which indicates that CF presents a large proportion of pores of size below 0.5 nm. Therefore, the presence of phosphorus avoids the mesopores development by oxidation but generates wider microporosity than P-free lignin-based carbon fibers.

Table 3 reports the elemental surface mass concentration obtained by XPS. As explained before, PCFs are more capable of taking oxygen than CFs due to the presence of phosphorus surface groups (e.g., C–O–PO₃ like groups), so oxygen mass surface concentration is higher in phosphorus-containing fibers (PCFs). Similar results have been observed for other carbonaceous materials activated with H_3PO_4 [24,43,44]. The decrease in oxygen mass surface concentration in CFs with the increase in the platinum content can be assigned to the gasification reaction that occurs during the carbonization stage, where oxygen is removed as CO or CO_2 . According to XPS analyses, it is easy to control the amount of phosphorus in the final carbon fibers (Table 3).

Fig. 2 displays the Pt4f and O1s spectra for the different carbon fibers (spectra are normalized to have a better visual comparison). The Pt4f region of the spectra presents a doublet corresponding to Pt4f_{7/2} and Pt4f_{5/2} respectively [45]. The separation between peaks, due to spin orbital splitting, is a quantized value of 3.33 eV. The Pt4f peak can be deconvoluted into two contributions. The Pt4f_{7/2} peak at around 71.5 eV can be attributed to Pt⁰, while the Pt4f_{7/2} peak located at around 73.0 eV is related to Pt²⁺ [45]. PCFs do not show significant modifications in the platinum species ratio (about 65 wt% of Pt⁰), whereas the amount of metallic platinum increases when increasing the total platinum mass in CFs. Interestingly, the amount of Pt²⁺ is higher for PCFs.

O1s spectra show a well-defined maximum located at 532.2 eV that can be attributed to C–O single bond. In comparison with CFs, PCFs exhibit a higher intensity of the hump corresponding to combined platinum (Pt–O) at 529.8 eV, due to the higher presence of Pt²⁺–oxygen species.

Fig. 3 shows the variation of carbon, oxygen, phosphorus and platinum species concentration during the preparation of the final CFHPT and PCFHPT electrodes: just after being electrospun (as-spun), after stabilization stage in air and after carbonization stage at 900 °C. The loss of volatile compounds and oxygen groups explains the increase in carbon concentration and the decrease in oxygen in the carbonization stage (Fig. 3a and b). Pt²⁺ concentration is similar in the two first stages (as-spun and after stabilization), being the platinum ratio (Pt²⁺/Pt⁰) c.a. 60/40 in both, CFHPT and PCFHPT.

As shown in Fig. 3c, the platinum ratio after carbonization stage is 13/87 (Pt²⁺/Pt⁰) for CFHPT, involving an important increase in the metallic species. The suggested oxygen transfer between platinum and carbon may explain this result. Thus, Pt²⁺ is reduced to the

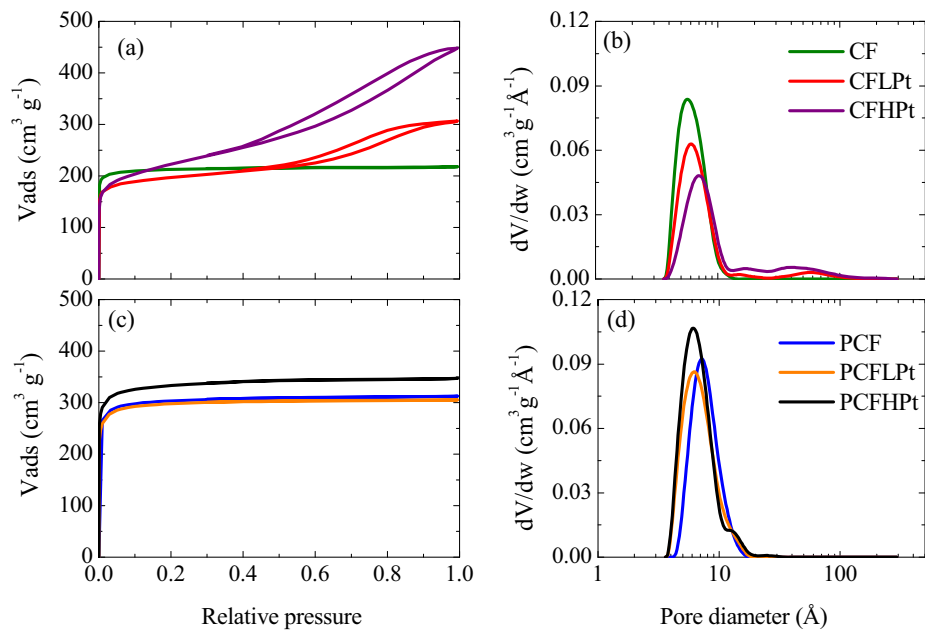


Fig. 1. N₂ adsorption–desorption isotherms at –196 °C of (a) CFs and (c) PCFs. Pore size distribution of (b) CFs and (d) PCFs.

Table 2
Porous textural parameters of the carbon fibers.

Sample	N ₂ isotherm				CO ₂ isotherm	
	A _{BET} (m ² g ⁻¹)	A _t (m ² g ⁻¹)	V _t (cm ³ g ⁻¹)	V _{mes} (cm ³ g ⁻¹)	A _{DR} (m ² g ⁻¹)	V _{DR} (cm ³ g ⁻¹)
CF	851	8	0.33	0.01	1002	0.40
CFLPt	747	161	0.23	0.24	729	0.30
CFHPT	786	383	0.18	0.51	618	0.25
PCF	1210	14	0.47	0.01	1017	0.41
PCFLPt	1159	11	0.46	0.01	1007	0.40
PCFHPT	1289	29	0.51	0.02	1158	0.46

Table 3
Mass surface concentration obtained by XPS quantitative analysis and CO and CO₂ evolved from TPD analyses.

Sample	XPS				TPD	
	C (wt%)	O (wt%)	P (wt%)	Pt (wt%)	CO (mg g ⁻¹)	CO ₂ (mg g ⁻¹)
CF	95.9	4.1	–	–	68.3	12.7
CFLPt	95.1	3.9	–	1.0	41.8	19.9
CFHPT	90.4	2.5	–	7.1	97.2	14.3
PCF	90.5	7.3	2.2	–	98.5	15.4
PCFLPt	87.6	7.8	2.3	2.3	202.1	28.1
PCFHPT	75.0	11.4	2.4	11.2	152.7	44.5

metallic form, and carbon takes the oxygen, which leads to carbon gasification and to the development of mesopores in CFHPT. This carbon gasification during the carbonization stage also explains the important oxygen mass surface concentration drop (Fig. 3a) in comparison to that of PCFHPT. On the other hand, PCFHPT exhibits a change of the platinum ratio from 60/40 to 30/70 approximately (Fig. 3d) during the carbonization stage. Therefore, part of platinum reduces its oxidation state but carbon does not undergo a significant oxidation reaction, since this carbon fiber does not develop mesopores. This result suggests that the presence of phosphorus changes the mechanism of the carbon oxidation reaction [43]. In this case, surface phosphorus groups take the oxygen that Pt²⁺ loses, allowing the metal reduction and inhibiting the carbon oxidation. For this reason, oxygen represents more than 11 wt% (Fig. 3b) of the final PCFHPT, which remains most of it combined with phosphorus, forming stable phosphate anions (C–O–P–O[–] and C–P–O[–]). The higher platinum ratio (Pt²⁺/Pt⁰) in P-containing carbon fiber

is probably due to a strong interaction between Pt²⁺ and these P-anions.

TPD analysis was used to identify the oxygen surface groups of the carbon fibers. Table 3 reports the amount of CO and CO₂ evolved from TPD of the carbon fibers up to a final temperature of 930 °C. Oxygen surface groups with acid character such as carboxylic and lactonic evolve as CO₂ upon thermal desorption. Carbonyl, ether, phenolic and quinone carbon–oxygen surface groups evolve as CO at higher temperature, while anhydride evolves as both CO and CO₂ [46]. As can be seen in Table 3, the amount of desorbed CO is higher than the amount of CO₂, what means that carbon–oxygen groups of acid character are minority on the carbon fibers surface. According to previous research, this fact usually happens when the carbonization temperature is higher than 600 °C [47].

An increase in the evolution of oxygen (mainly as CO) has been observed in PCFs (Table 3) at higher temperatures than 800 °C, which has been previously assigned to the decomposition of stable

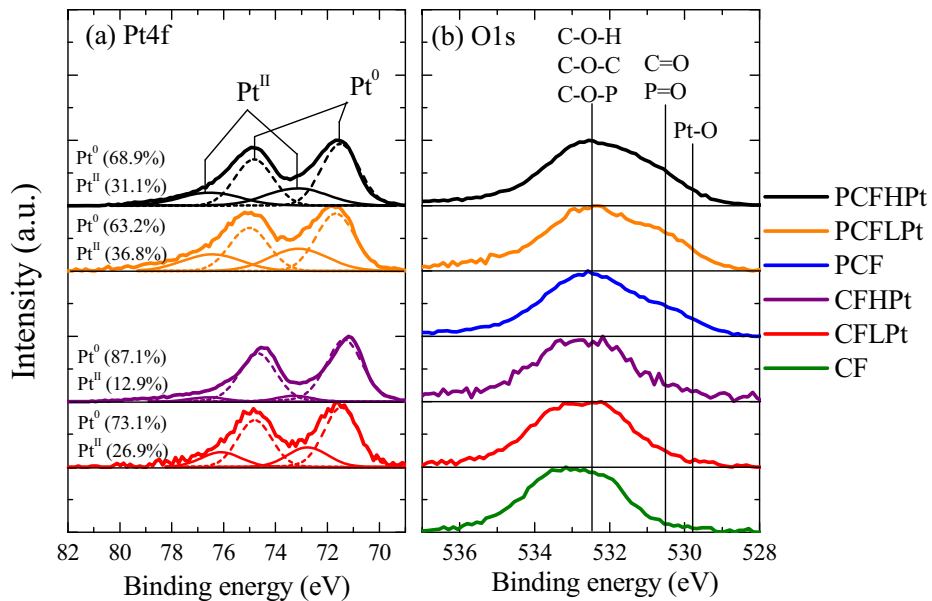


Fig. 2. (a) Pt4f and (b) O1s XPS spectra for the carbonized fibers with and without phosphorus.

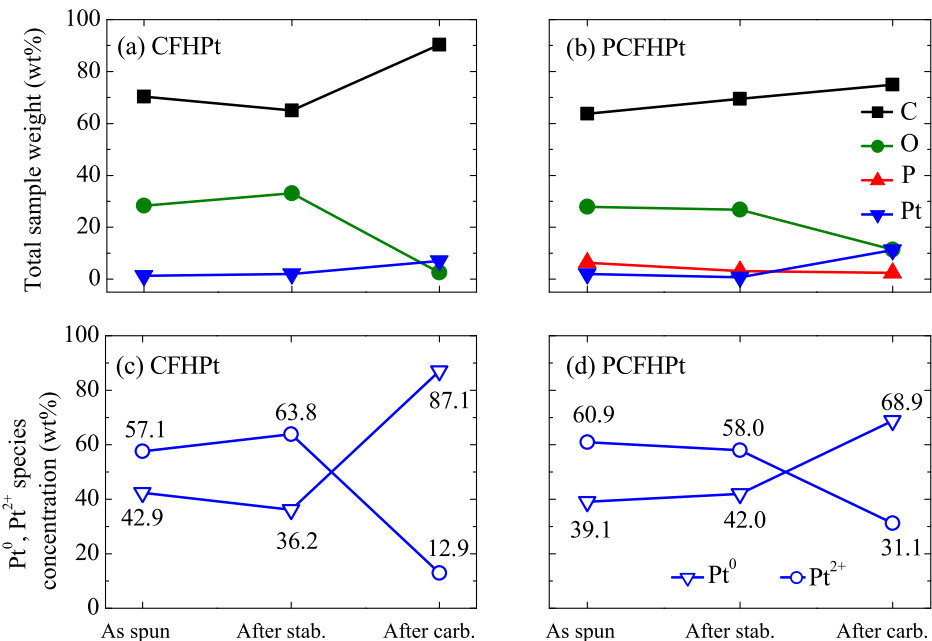


Fig. 3. C, O, P and Pt mass surface concentration obtained by XPS quantitative analysis for as-spun, stabilized and carbonized (a) CFHpt and (b) PCFHpt, and evolution of Pt⁰ and Pt^{II} species concentration in (c) CFHpt and (d) PCFHpt.

C–O–P–O surface groups to produce C–P–O [42,48]. The CO₂ evolution observed in these fibers at these high temperatures could be due to CO-evolved secondary reactions with other surface oxygen groups [49], in part catalyzed by the presence of platinum in PCFLPt and PCFHpt.

Phosphorus groups of carbonaceous materials provide the fibers with a regular and non-defect surface with small platinum nanoparticles, as shown in SEM and TEM micrographs (Fig. 4). General fiber morphology is shown in Fig. 4a and b where SEM micrographs are represented. Melting of fibers is avoided due to the thermostabilization treatment applied to the as-spun material [39]. Non-interconnected fibers are displayed in Fig. 4a and b, corresponding to CFHpt and PCFHpt respectively, in spite of the faster thermostabilization process of PCFs. The fibers diameter obtained

by this preparation method is between 600 nm and 1 μ m for CFs, whereas fiber sizes from 600 nm to 3 μ m are observed when phosphoric acid is added to the spinnable solution (PCFs).

Electrospinning method allows for obtaining a good distribution of platinum nanoparticles in the fibers as all TEM images show (Fig. 4c–f) and it was previously reported [28,50]. Phosphorus-containing fibers present a smaller Pt particle size (see bar length) than those of the homologous fibers without phosphorus. The larger particle size of Pt on CFHpt (Fig. 4e) could be related to the formation of mesopores and the decrease in the carbonization yields (Fig. 1a and Table 1). This way, the Pt-promoted gasification of the carbon surface during the thermal stages facilitates the migration and sintering of platinum particle, reducing the metallic specific area. On the other hand, the inhibition of carbon oxidation in PCFs and the

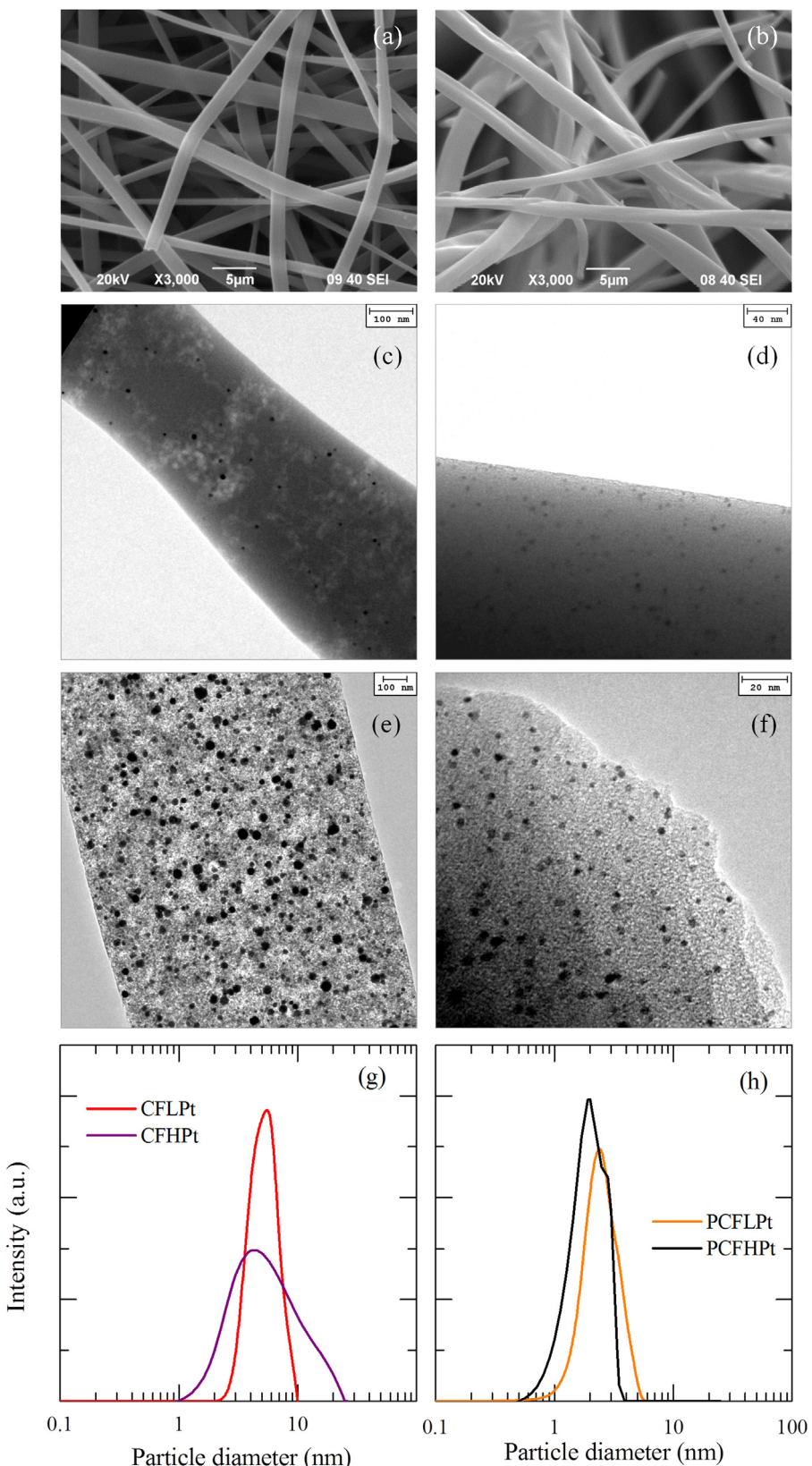


Fig. 4. SEM and TEM images of carbon fibers electrocatalysts. SEM micrographs of (a) CFHPt and (b) PCFHPt; TEM images of (c) CFLPt, (d) CFHPt, (e) PCFLPt and (f) PCFHPt; Pt particle size distribution of (g) CFLPt, CFHPt, (h) PCFLPt and PCFHPt.

interaction of Pt^{2+} with P-anions, observed by XPS analysis, restrict this Pt migration, yielding smaller and well-dispersed Pt particles. This improvement of Pt dispersion has been previously observed in P-containing carbonaceous materials [51].

As shown in Fig. 4g and h, the particle size distributions of CFs are wider than those for PCFs. The average particle size, which has been estimated from the particle size distribution, is similar for PCFLPt and PCFHPT (2.8 and 2.1 nm respectively). On the other hand, the increase in the surface oxidation of CFs (developing mesopores) leads to higher Pt particle sizes (5.6 nm for CFLPt and 9.6 nm for CFHPT).

Fig. 4e shows an apparent higher Pt concentration than the one determined by XPS analysis (Table 3). TEM images allow for observing the total amount of platinum in the studied region, while XPS analysis only determines the surface concentration (around 20 Å deep). The total concentration of platinum in carbon fibers can also be calculated by a mass balance of platinum in the fibers, attending to the overall yield in thermal stages and considering no platinum losses during thermal processes. On one hand, similar Pt concentrations are obtained from XPS and from mass balance in CFs, indicating the uniform distribution of Pt in the carbon fibers. On the other hand, higher Pt content is shown in PCFs from XPS analysis when these values are compared with that calculated in the bulk. This result suggests that Pt is mainly located in the most external fiber surface in these cases. This phenomenon can be related to the P-groups behavior during the thermal stage, which could retain the metal in the external surface of the fibers.

Carbon fibers were submitted to TG analyses in air atmosphere for comparing the fiber behavior and the platinum activity with and without phosphorus (Fig. 5). Platinum-free fibers show similar behavior than the ones previously reported for activated carbons with H_3PO_4 [43,44]. Phosphorus makes fibers more resistant to oxidation, and platinum tends to decrease the temperature at which oxidation reaction begins (about 50 °C and 100 °C for low and high Pt content, respectively).

As previously discussed, phosphorus makes carbon resistant to oxidation in poor-oxygen atmosphere (carbonization conditions) in spite of platinum presence (see the carbonization yields in Table 1). Nevertheless, an opposite behavior is observed in oxygen-rich atmosphere (combustion conditions). The promotion of the onset combustion temperature of PCFLPt and PCFHPT (vs. their counterparts) suggests that phosphorus enhances the platinum activity as it acts as oxygen donor. However, TG analysis proved that carbon–phosphorus surface groups are very stable and it is necessary to submit the fiber to higher combustion temperature to oxidize the entire carbon surface. Comparing the 3

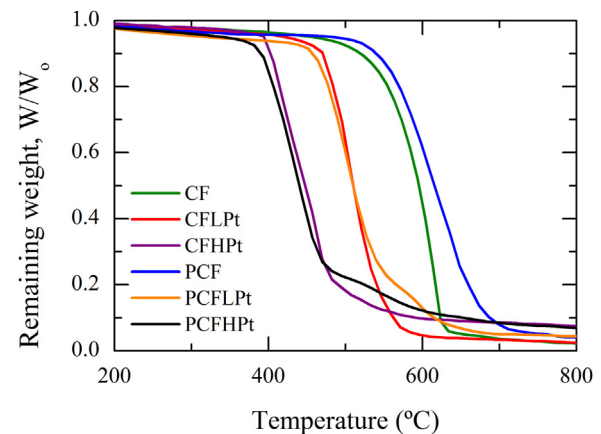


Fig. 5. Non isothermal oxidation profiles of CFs and PCFs.

pairs of TG curves, PCFs need higher temperature than the corresponding CFs (with the same platinum composition) to burn-off all the carbon. These stable phosphorus groups present a maximum in TPD curves at high temperatures, corresponding to C–O–P surface groups decomposition, as reported in previous researches [40,48,52].

3.3. Electrochemical characterization and alcohol electro-oxidation

The electrochemical characterization was carried out in a three electrode cell by using the obtained lignin-based CFs and PCFs as electrodes without any conductivity promoter and binder. Fig. 6 displays the voltammograms, within the stability potential window, in acid electrolyte of the different lignin-based carbon fibers prepared in this work. The anodic current rise at higher positive potentials has been related to the electro-oxidation of carbon and/or the oxygen evolution reaction (OER); whereas the increase in the cathodic current at negative potentials mainly seems to correspond with the hydrogen evolution reaction (HER). This HER is highly reversible on Pt, so that the anodic peaks in the potential region between -0.2 V and 0.0 V observed for Pt-containing samples are due to the oxidation of the generated H_2 on this electrocatalyst. Accordingly, the observation of these peaks suggests that the Pt nanoparticles in the different lignin-based CFs and PCFs are accessible to the electrolyte and electro-active.

The presence of phosphorus in the fibers (Fig. 6b) yields carbon electrodes with a larger double-layer charge, which can be

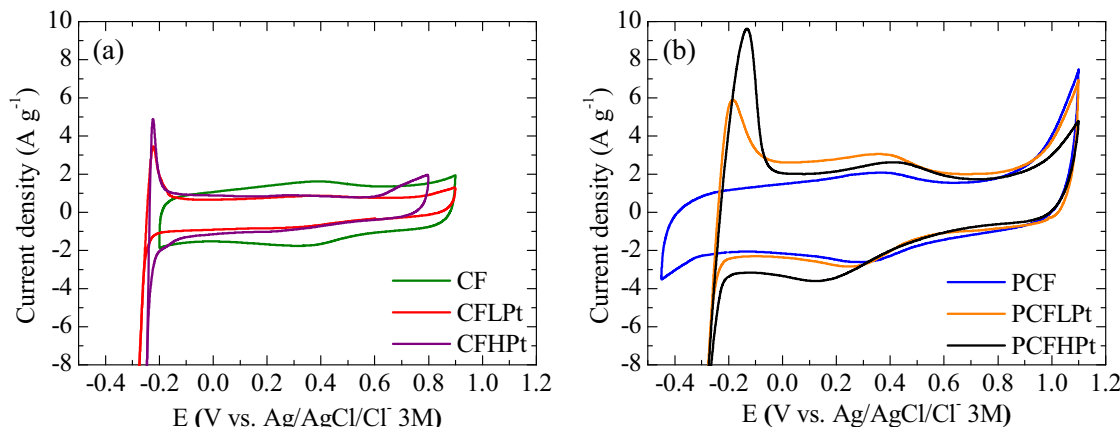


Fig. 6. Cyclic voltammograms up to different upper limit potentials (1st cycle) of (a) CFs and (b) PCFs electrodes with variable Pt content in the absence of methanol. 0.5 M H_2SO_4 ; $v = 10 \text{ mV s}^{-1}$.

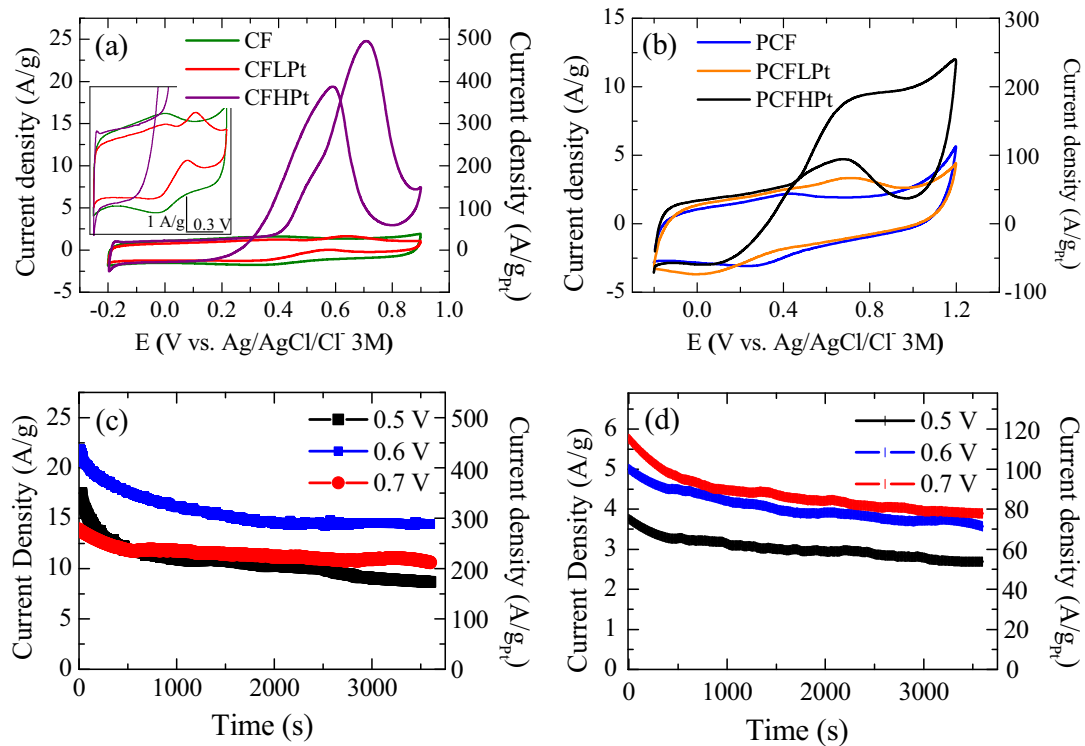


Fig. 7. Steady cyclic voltammograms of (a) CFs and (b) PCFs electrodes with variable Pt content in the presence of methanol ($v = 10 \text{ mV s}^{-1}$). Chronoamperometric measurements for methanol electro-oxidation at different potentials on (c) CFHPt and (d) PCFHPt. Electrolyte 0.5 M H_2SO_4 + 1.5 M methanol.

related to their larger surface area and/or volume of wider micropores (Table 2) accessible to the electrolyte ions. On the other hand, the voltammograms of the different electrodes also contain a more or less reversible broad peak centered at around 0.4 V. This peak is attributed to faradic processes involving quinone-like oxygen groups on carbon surfaces [53] and it is more intense in PCFs electrodes, in agreement with their higher content in CO-evolving groups (Table 3).

Regarding the electrochemical stability, in the absence of P (Fig. 6a), the electrode without Pt (CF) started to suffer from electro-oxidation [54] above ca. 0.9 V (vs. Ag/AgCl/Cl⁻ (3 M)). This oxidation potential can be considered slightly high when compared to conventional activated carbons [24], and may be associated to the suitable structure of carbon electrodes prepared from lignin [13]. On the other hand, the electro-oxidation resistance of the fibers was further enhanced with the incorporation of P (PCF), with an onset potential from 1.1 V (Fig. 6b). This inhibition of carbon electro-oxidation in PCFs is in agreement with the higher oxidation resistance observed in O_2 atmosphere (Fig. 5), and can be uniquely assigned to the slower oxidation of carbon mediated by phosphorus surface functionalities [24].

As it can be observed in Fig. 6a, the introduction of Pt on CFs without P remarkably decreases their electro-oxidation onset potential down to ca. 0.75 and 0.6 V for the fibers with low and high Pt content, respectively. This is due to the well-known electrocatalytic activity of Pt for carbon oxidation and oxygen evolution reaction [55]. However, in the presence of P (Fig. 6b), this effect decreases independently of the studied Pt content. This result indicates that P surface groups could protect carbon against electro-oxidation, even when it is acting as electrocatalyst support, and that Pt electrocatalysts activity for oxygen evolution reaction is strongly decreased.

In the region of lower potentials, Pt causes a decrease in the overpotential and an increase in the cathodic current density for the HER (Fig. 6a and b). In particular, the onset potential for HER in the

carbon fibers without P is shifted from -0.30 (CF) to -0.15 V for the high Pt concentration (CFHPt). Nevertheless, the P surface groups were found to affect also the HER. In this sense, from the comparison of Fig. 6a with b it can be clearly deduced that the HER overpotential for the fibers with P and variable Pt content (Fig. 6b) are at least 0.1 V higher than that of the corresponding electrodes without P (Fig. 6a). This indicates that P surface groups are also affecting the activity of Pt species although this effect is much less relevant than at positive potentials [56]. These results are extremely interesting and reflect the effect of P on the Pt reducibility as observed by XPS. Upon positive polarization P-functional groups remain oxidized or can be fully oxidized what favors the interaction with Pt²⁺ species which will not be reduced and will have a low activity toward oxidation reaction either of the support or the electrolyte. On the other hand, at negative potentials P-groups can be reduced (especially in presence of a catalyst like Pt) what will remove the impediment for further Pt²⁺ species reduction which will contribute to the reaction occurring at these negative potential conditions.

The conductivity and stability shown by the different lignin-based carbon fibers make these electrodes auspicious electrocatalysts for electro-oxidizing several compounds in aqueous solution. In such a way, the electrocatalytic behavior of these electrodes has been studied for the methanol and ethanol oxidation reactions (MOR and EOR, respectively), which are well-known important processes in fuel cells for energy conversion [57,58]. Fig. 7a and b display the voltammetric response of the CF electrodes without (Fig. 7a) and with P (Fig. 7b) and variable Pt content in the presence of methanol. Independently of the presence of P, the electrodes without Pt (samples CF and PCF) showed a CV profile quite similar to those obtained in an electrolyte solution free of methanol. And the same result was found in the case of ethanol (Fig. not shown). This indicates that without Pt, the lignin-based carbon fibers electrodes present no electro-activity for MOR or EOR.

By contrast, the electrodes exhibited an outstanding alcohol electro-oxidation performance when Pt was introduced in the car-

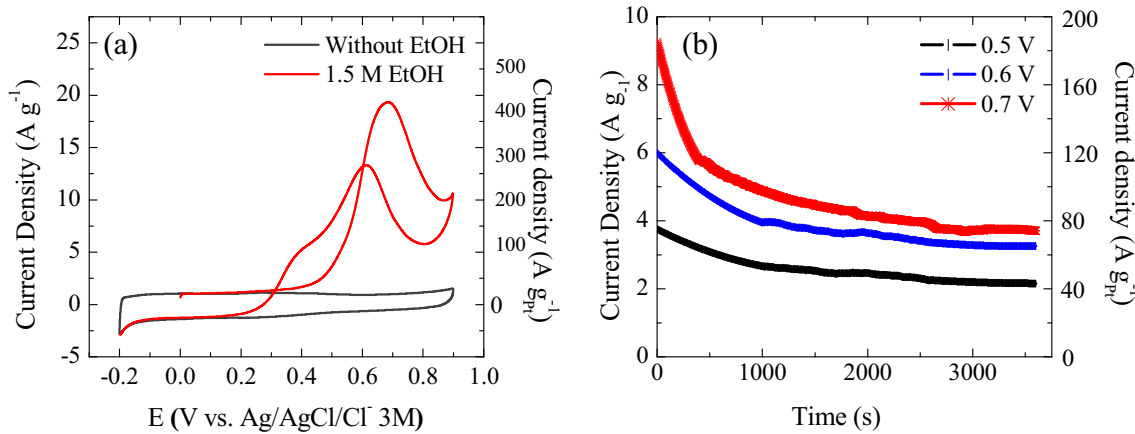


Fig. 8. (a) Steady cyclic voltammograms of CFHPt electrode in the presence or absence of EtOH ($v = 10 \text{ mV s}^{-1}$). (b) Chronoamperometric measurements for EtOH electro-oxidation at different potentials on CFHPt electrode. Electrolyte $0.5 \text{ M H}_2\text{SO}_4 + 1.5 \text{ M EtOH}$.

Table 4
Comparison of CFHPt sample activity with data in the literature.

$j \text{ (A g}^{-1}\text{)}_{\text{Pt}}$	Nominal metal content (wt%)	Alcohol conc. (M)	Electrolyte	Reference
<i>Methanol oxidation</i>				
495	Pt (5)	1.5	$0.5 \text{ M H}_2\text{SO}_4$	CFHPt (this work)
300	PtRu (20)	2	$0.5 \text{ M H}_2\text{SO}_4$	[65]
260	PtRu (30)	2	$0.5 \text{ M H}_2\text{SO}_4$	[66]
215	Pt (5)	1	$1 \text{ M H}_2\text{SO}_4$	[67]
91	Pt (20)	1	$1 \text{ M H}_2\text{SO}_4$	[67]
73	Pt (20)	1	$1 \text{ M H}_2\text{SO}_4$	[67]
86	Pt (electrodeposited)	0.1	$0.5 \text{ M H}_2\text{SO}_4$	[68]
275	Pt (20)	0.1	$0.5 \text{ M H}_2\text{SO}_4$	[69]
<i>Ethanol oxidation</i>				
370	Pt (5)	1.5	$0.5 \text{ M H}_2\text{SO}_4$	CFHPt (this work)
125	Pt (40)	1	0.1 M HClO_4	[70]
180	Pt (20)	1	$0.5 \text{ M H}_2\text{SO}_4$	[71]

bon fibers. In the absence of P (Fig. 7a), both CFLPt and CFHPt electrodes display two defined anodic peaks, in the forward and reverse scans, respectively, characteristic of methanol oxidation on Pt via the so-called “dual-path” mechanism [59]. The oxidation process in the forward scan has been assigned to “the active intermediate reaction path”, in which adsorbed methanol and intermediates are oxidized directly by O-containing species on Pt to form CO₂. In the reverse scan, the anodic peak is related to the “poisoning intermediate reaction path”, i.e., the removal of the incompletely oxidized carbonaceous species formed in the forward scan, mostly in the form of CO bonded to Pt. Nevertheless, it has been recently proposed that the origin of this second oxidation peak is the methanol oxidation on platinum oxides (Pt–O_x) [60]. In the case of CFLPt, the peak currents of the forward and reverse peaks were found at 0.65 and 0.57 V, respectively; whereas they appeared at 0.71 and 0.59 V increasing the amount of Pt (CFHPt).

The effect of Pt content on methanol oxidation was particularly remarkable when comparing the oxidation onset potentials and current densities of both electrodes. As it can be observed in Fig. 7a, the fibers with lower Pt content (CFLPt) start to oxidize methanol at ca. 0.35 V, producing a maximum current density in the forward scan (I_f) close to 1.7 A g^{-1} . On the other hand, for CFHPt electrode the oxidation onset potential is ca. 0.25 V and the reaction produces a prominent anodic peak with I_f up to 25 A g^{-1} . Considering the content of Pt electrocatalyst (active phase) on the electrodes (nominal Pt contents), and after correction of the double-layer charge, the values of I_f can be calculated as 75 and $495 \text{ A g}^{-1} \text{ (Pt)}$ for CFLPt and CFHPt, respectively.

Regarding the mentioned “dual-path” mechanism, the ratio of the forward (I_f) to the reverse (I_b) anodic peak current densities, I_f/I_b , can be used to describe the catalyst tolerance to carbonaceous species accumulation [61]. The electrocatalytic response and, therefore, the I_f/I_b ratio for the different electrodes was remarkably stable upon cycling (see Supp. Info., Fig. S1). For the CFLPt and CFHPt electrodes, the calculated I_f/I_b values are 0.6 and 1.2, respectively. This last high I_f/I_b ratio indicates excellent oxidation of methanol to CO₂ during the anodic scan and poor accumulation of intermediates on the Pt surface [61].

With respect to the role of P, Fig. 7b shows that Pt-containing PCFs electrodes present also a good electro-activity for methanol electro-oxidation. However, their performance is significantly lower when compared to that of the corresponding electrodes without P (Fig. 7a). This seems to be consequence of the Pt interaction with P-functional groups that results in different degree of Pt reducibility as has been previously discussed. The PCFLPt starts to oxidize methanol at ca. 0.4 V and the forward oxidation reaches a maximum of 3.3 A g^{-1} at 0.71 V. Particularly, and probably due to the large double-layer currents, the reverse oxidation peak is poorly defined in this case. This response was greatly improved when a higher Pt content was introduced in the fibers. Thus, PCFHPt oxidized methanol from ca. 0.35 V, entailing considerably broader forward and reverse oxidation peaks. The forward peak presents a less-defined maximum at 0.79 V with a current density of 9.5 A g^{-1} . Interestingly, PCFHPt electrode can effectively electro-oxidize methanol at higher potentials, between 0.9 and 1.1 V, where, unlike in the case of CFs without P, neither carbon nor electrolyte electro-oxidation reactions occur (Fig. 6b). In the

reverse scan, the maximum is observed at 0.67 V and the current density reaches 4.7 A g^{-1} . Expressed in terms of Pt mass, the values of I_f can be calculated as 130 and $170 \text{ A g}^{-1}(\text{Pt})$ for PCFLPt and PCFHPT, respectively, and the I_f/I_b ratio for the PCFHPT electrode is 1.1, which again reflects a good activity toward complete methanol oxidation during the anodic scan.

The electro-oxidation of methanol was further studied at constant electrode potential. Fig. 7c and d display the chronoamperometric response of CFHPT and PCFHPT electrodes at various potentials in the presence of methanol. Among the electrodes with or without P, CFHPT and PCFHPT electrodes have been chosen for this study because of their higher activity for methanol oxidation. As it can be observed, independently of the applied potential, both electrodes show high oxidation currents that slightly decrease with time. Nevertheless, a 70–75% of the initial current is retained by both electrodes in the first hour of experiment. This current decay has been generally observed in several electrocatalysts and has been related to a blockage of the surface by some organic residue and/or other deactivation mechanisms [62]. Particularly, the oxidation currents provided by the electrode without P are 3–5 times higher, what is in agreement with the voltammetric characterization. On the other hand, the influence of the applied potential on the oxidation currents seems to be different for both electrodes. Thus, in the case of CFHPT electrode (Fig. 7c), a remarkably higher maximum current is obtained when working at 0.6 V, while it gradually increases with the electrode potential for the PCFHPT electrode (Fig. 7d).

Finally, the electro-activity of the reported lignin-based carbon fibers was tested for ethanol electro-oxidation. Fig. 8a compares the voltammetric response of a CFHPT electrode in the presence or absence of ethanol. The onset for ethanol oxidation is observed at ca. 0.25 V and, as in the case of methanol, the voltammogram shows two clear oxidation peaks in the forward and reverse scans, respectively. In the forward scan the current reaches a maximum of 19.4 A g^{-1} ($I_f = 370 \text{ A g}^{-1}(\text{Pt})$) at 0.69 V, whereas it reaches 13.4 A g^{-1} ($I_b = 290 \text{ A g}^{-1}(\text{Pt})$) at 0.61 V in the reverse scan. This electrode exhibits, then, an $I_f/I_b = 1.26$ for ethanol oxidation. Again, the high oxidation currents as well as the high I_f/I_b ratio are indicative of an excellent electrocatalytic performance.

Under potentiostatic conditions (Fig. 8b), the CFHPT electrode exhibits high oxidation currents that increase with the electrode potential. These ethanol oxidation currents gradually decay with time, so that a 40–60% of the initial current is obtained after 1 h-experiments. The activity loss increases with the electrode potential and is larger than in the case of methanol. Nevertheless, the observed steady currents range high from 40 to $80 \text{ A g}^{-1}(\text{Pt})$.

Although any comparison with vast literature is difficult (because of the multiple different preparation methods and characterization conditions and protocols used by other authors) [29,57,63,64], we have tried to compare our results with some data in the literature (Table 4). Regarding the values of current density ($\text{A g}^{-1}(\text{Pt})$), it is noteworthy that the CFHPT electrodes studied in the present work exhibit an outstanding performance for methanol and ethanol oxidation: low onset potential, and high specific oxidation currents and I_f/I_b ratios as well as stable catalytic response. Probably, the excellent platinum distribution and high dispersion are the main factors that explain this good activity. On the other hand, the presence of P decreases the catalytic performance of these electrodes, but they increase the electro-oxidation resistance of the carbon support. Moreover, regarding the Pt (active phase) morphology after MOR and EOR, TEM images (not shown) reveal that both nanoparticle size and dispersion are quite similar to those exhibited by the initial carbon electrodes (with and without P). Thereby, no particle migration or sintering is observed during the alcohol electro-oxidation, which confirms the great stability of these Pt-containing carbon fibers as electrocatalysts. All

these features make the reported lignin-based carbon fibers, which have been prepared by an advantageous procedure, promising low-Pt content electrodes for fuel cell technology. This is an important result since suitable low-Pt content catalysts are necessary for the up-coming large scale commercialization of different types of fuel cells [57].

4. Conclusions

Lignin fiber, with and without phosphorus surface groups and platinum nanoparticles, were synthesized in a single step by electrospinning lignin/ethanol/phosphoric acid/platinum acetylacetone precursor solutions. The different lignin fibers thus obtained were stabilized in air atmosphere and carbonized at 900 °C in nitrogen atmosphere in order to obtain lignin-based carbon fiber electrocatalysts. Phosphorus groups allow a 10 times faster heating rate (0.08 °C min^{-1} vs. 0.8 °C min^{-1} with phosphorus) and a decrease of the isothermal stabilization step 100 times (100 h and 1 h) to avoiding fibers melting. Phosphorus-containing carbon fibers obtained are microporous solids that can develop an apparent surface area of $1141 \text{ m}^2 \text{ g}^{-1}$, whereas lignin-based carbon fibers without phosphorus present wide mesoporosity and apparent surface areas lower than $780 \text{ m}^2 \text{ g}^{-1}$. Phosphorus groups allow the preparation of catalysts with very well dispersed metallic nanoparticles (about 2 nm) while without phosphorus larger Pt particle sizes are obtained. Better oxidation and electrooxidation resistance have been shown by carbon fibers with phosphorus. The obtained Pt-containing carbon fibers can be directly used as electrodes with no binder or conductivity promoter, showing a remarkable electrocatalytic response in the methanol and ethanol electro-oxidation reactions. Cyclic voltammograms displays two defined anodic peaks for these electrocatalysts and, in both reactions, they exhibit relatively low onset potential, high specific oxidation currents and a stable catalytic response.

Acknowledgment

This work was supported by the Spanish MINECO under CTQ2015-68654-R project.

Appendix A. Supplementary data

Supplementary data associated with this article can be found, in the online version, at <http://dx.doi.org/10.1016/j.apcatb.2017.04.008>.

References

- [1] R. Sahay, P.S. Kumar, R. Sridhar, J. Sundaramurthy, J. Venugopal, S.G. Mhaisalkar, et al., Electrospun composite nanofibers and their multifaceted applications, *J. Mater. Chem.* 22 (2012) 12953.
- [2] M. Zhang, A.A. Ogale, Carbon fibers from dry-spinning of acetylated softwood kraft lignin, *Carbon* 69 (2014) 626–629.
- [3] E. Frank, L.M. Steudle, D. Ingildeev, J.M. Spörli, M.R. Buchmeiser, Carbon fibers: precursor systems, processing, structure, and properties, *Angew. Chem. Int. Ed.* 53 (2014) 5262–5298.
- [4] P.T. Williams, A.R. Reed, Development of activated carbon pore structure via physical and chemical activation of biomass fibre waste, *Biomass Bioenergy* 30 (2006) 144–152.
- [5] J.F. Kadla, S. Kubo, R.A. Venditti, R.D. Gilbert, A.L. Compere, W. Griffith, Lignin-based carbon fibers for composite fiber applications, *Carbon* 40 (2002) 2913–2920.
- [6] J.M. Rosas, R. Berenguer, M.J. Valero-Romero, J. Rodríguez-Mirasol, T. Cordero, Preparation of different carbon materials by thermochemical conversion of lignin, *Front. Mater.* 1 (2014) 29.
- [7] L.M. Cotoruelo, M.D. Marqués, A. Leiva, J. Rodríguez-Mirasol, T. Cordero, Adsorption of oxygen-containing aromatics used in petrochemical, pharmaceutical and food industries by means of lignin based active carbons, *Adsorption* 17 (2011) 539–550.
- [8] L.M. Cotoruelo, M.D. Marqués, J. Rodríguez-Mirasol, J.J. Rodríguez, T. Cordero, Lignin-based activated carbons for adsorption of sodium dodecylbenzene

sulfonate: equilibrium and kinetic studies, *J. Colloid Interface Sci.* 332 (2009) 39–45.

[9] J. Bedia, R. Barrionuevo, J. Rodríguez-Mirasol, T. Cordero, Ethanol dehydration to ethylene on acid carbon catalysts, *Appl. Catal. B Environ.* 103 (2011) 302–310.

[10] J. Bedia, J.M. Rosas, J. Rodríguez-Mirasol, T. Cordero, Pd supported on mesoporous activated carbons with high oxidation resistance as catalysts for toluene oxidation, *Appl. Catal. B Environ.* 94 (2010) 8–18.

[11] M. Funaoka, Lignin: its functions and successive flow, *Macromol. Symp.* 201 (2003) 213–221.

[12] D. Yawalata, L. Paszner, Anionic effect in high concentration alcohol organosolv pulping, *Holzforschung* 58 (2005) 1–6.

[13] R. Berenguer, F.J. García-Mateos, R. Ruiz-Rosas, D. Cazorla-Amorós, E. Morallón, J. Rodríguez-Mirasol, et al., Biomass-derived binderless fibrous carbon electrodes for ultrafast energy storage, *Green Chem.* 18 (2016) 1506–1515.

[14] R.R. Salunkhe, S.H. Hsu, K.C.W. Wu, Y. Yamauchi, Large-scale synthesis of reduced graphene oxides with uniformly coated polyaniline for supercapacitor applications, *ChemSusChem* 7 (2014) 1551–1556.

[15] R.R. Salunkhe, C. Young, J. Tang, T. Takei, Y. Ide, N. Kobayashi, et al., A high-performance supercapacitor cell based on ZIF-8-derived nanoporous carbon using an organic electrolyte, *Chem. Commun.* 52 (2016) 4764–4767.

[16] W. Zhou, Z. Zhou, S. Song, W. Li, G. Sun, P. Tsikararas, et al., Pt based anode catalysts for direct ethanol fuel cells, *Appl. Catal. B Environ.* 46 (2003) 273–285.

[17] A.M. Zainuddin, S.K. Kamarudin, M.S. Masdar, W.R.W. Daud, A.B. Mohamad, J. Sahari, High power direct methanol fuel cell with a porous carbon nanofiber anode layer, *Appl. Energy* 113 (2014) 946–954.

[18] M. Sevilla, C. Sanchís, T. Valdés-Soh, E. Morallón, A.B. Fuertes, Synthesis of graphitic carbon nanostructures from sawdust and their application as electrocatalyst supports, *J. Phys. Chem. C* 111 (2007) 9749–9756.

[19] M. Sevilla, C. Sanchís, T. Valdés-Solís, E. Morallón, A.B. Fuertes, Direct synthesis of graphitic carbon nanostructures from saccharides and their use as electrocatalytic supports, *Carbon* 46 (2008) 931–939.

[20] J.M. Sieben, A. Ansón-Casaos, M.T. Martínez, E. Morallón, Single-walled carbon nanotube buckypapers as electrocatalyst supports for methanol oxidation, *J. Power Sources* 242 (2013) 7–14.

[21] J. Tang, J. Liu, N.L. Torad, T. Kimura, Y. Yamauchi, Tailored design of functional nanoporous carbon materials toward fuel cell applications, *Nano Today* 9 (2014) 305–323.

[22] D. Hulicova-Jurcakova, M. Seredych, G.Q. Lu, N.K.A.C. Kodiweera, P.E. Stallworth, S. Greenbaum, et al., Effect of surface phosphorus functionalities of activated carbons containing oxygen and nitrogen on electrochemical capacitance, *Carbon* 47 (2009) 1576–1584.

[23] D. Hulicova-Jurcakova, M. Kodama, S. Shiraishi, H. Hatori, Z.H. Zhu, G.Q. Lu, Nitrogen-enriched nanoporous carbon electrodes with extraordinary supercapacitance, *Adv. Funct. Mater.* 19 (2009) 1800–1809.

[24] R. Berenguer, R. Ruiz-Rosas, A. Gallardo, D. Cazorla-Amorós, E. Morallón, H. Nishihara, et al., Enhanced electro-oxidation resistance of carbon electrodes induced by phosphorus surface groups, *Carbon* 95 (2015) 681–689.

[25] X. Xu, J. Zhou, L. Jiang, G. Lubineau, S.A. Payne, Lignin-based carbon fibers: carbon nanotube decoration and superior thermal stability, *Carbon* 80 (2014) 91–102.

[26] N. Diez, P. Díaz, P. Álvarez, Z. González, M. Granda, C. Blanco, et al., Activated carbon fibers prepared directly from stabilized fibers for use as electrodes in supercapacitors, *Mater. Lett.* 136 (2014) 214–217.

[27] D. Sebastián, V. Baglio, M. Girolamo, R. Moliner, M.J. Lázaro, Aricò F.A.S., Carbon nanofiber-based counter electrodes for low cost dye-sensitized solar cells, *J. Power Sources* 250 (2014) 242–249.

[28] R. Ruiz-Rosas, J. Bedia, M. Lallave, I.G. Loscertales, A. Barrero, J. Rodríguez-Mirasol, et al., The production of submicron diameter carbon fibers by the electrospinning of lignin, *Carbon* 48 (2010) 696–705.

[29] M.A.F. Akhairi, S.K. Kamarudin, Catalysts in direct ethanol fuel cell (DEFC): an overview, *Int. J. Hydrogen Energy* 41 (2016) 4214–4228.

[30] Y. Lu, S. Du, R. Steinberger-Wilckens, One-dimensional nanostructured electrocatalysts for polymer electrolyte membrane fuel cells – a review, *Appl. Catal. B Environ.* 199 (2016) 292–314.

[31] J.W. Hong, Y. Kim, Y. Kwon, S.W. Han, Noble metal nanocrystals with controlled facets for electrocatalysis, *Chem. Asian J.* 11 (2016) 2224.

[32] L. Li, L. Hu, J. Li, Z. Wei, Enhanced stability of Pt nanoparticle electrocatalysts for fuel cells, *Nano Res.* 8 (2015) 418–440.

[33] J.N. Tiwari, R.N. Tiwari, G. Singh, K.S. Kim, Recent progress in the development of anode and cathode catalysts for direct methanol fuel cells, *Nano Energy* 2 (2013) 553–578.

[34] M. Lallave, J. Bedia, R. Ruiz-Rosas, J. Rodríguez-Mirasol, T. Cordero, J.C. Otero, et al., Filled and hollow carbon nanofibers by coaxial electrospinning of Alcell lignin without binder polymers, *Adv. Mater.* 19 (2007) 4292–4296.

[35] E. Leal da Silva, M.R. Ortega Vega, P. dos Santos Correa, A. Cuña, N. Tancredi, C. de Fraga Malfatti, Influence of activated carbon porous texture on catalyst activity for ethanol electro-oxidation, *Int. J. Hydrogen Energy* 39 (2014) 14760–14767.

[36] K. Kaneko, C. Ishii, T. Rybolt, Superhigh surface area determination of microporous carbons, *Stud. Surf. Sci. Catal.* 87 (1994) 583–592.

[37] M.M. Dubinin, E.D. Zaverina, L.D. Radushkevich, Sorption and structure of active carbon. I. Adsorption of organic vapors, *J. Phys. Chem. [URSS]* 21 (1947) 1351–1362.

[38] J. Jagiello, J.P. Olivier, 2D-NLDFT adsorption models for carbon slit-shaped pores with surface energetical heterogeneity and geometrical corrugation, *Carbon* 55 (2013) 70–80.

[39] J.L. Braun, K.M. Holtman, J.F. Kadla, Lignin-based carbon fibers: oxidative thermostabilization of kraft lignin, *Carbon* 43 (2005) 385–394.

[40] J. Bedia, J.M. Rosas, J. Márquez, J. Rodríguez-Mirasol, T. Cordero, Preparation and characterization of carbon based acid catalysts for the dehydration of 2-propanol, *Carbon* 47 (2009) 286–294.

[41] M. Jeguirim, K. Villani, J.F. Brilhac, J.A. Martens, Ruthenium and platinum catalyzed carbon oxidation: a comparative kinetic study, *Appl. Catal. B Environ.* 96 (2010) 34–40.

[42] J.M. Rosas, J. Bedia, J. Rodríguez-Mirasol, T. Cordero, HEMP-derived activated carbon fibers by chemical activation with phosphoric acid, *Fuel* 88 (2009) 19–26.

[43] J.M. Rosas, R. Ruiz-Rosas, J. Rodríguez-Mirasol, T. Cordero, Kinetic study of the oxidation resistance of phosphorus-containing activated carbons, *Carbon* 50 (2012) 1523–1537.

[44] M.J. Valero-Romero, F.J. García-Mateos, J. Rodríguez-Mirasol, T. Cordero, Role of surface phosphorus complexes in the oxidation of porous carbons, *Fuel Process. Technol.* 157 (2017) 116–126.

[45] J.F. Moulder, W.F. Stickle, P.E. Sobol, K.D. Bomben, *Handbook of X-ray Photoelectron Spectroscopy*, 1995.

[46] M. Calzado, M.J. Valero-Romero, P. Garriga, A. Chica, M.O. Guerrero-Pérez, J. Rodríguez-Mirasol, et al., Lignocellulosic waste-derived basic solids and their catalytic applications for the transformation of biomass waste, *Catal. Today* (2014) 4–11.

[47] E. Gonzalez-Serrano, T. Cordero, J. Rodriguez-Mirasol, L. Cotoruelo, J.J. Rodriguez, Removal of water pollutants with activated carbons prepared from H_3PO_4 activation of lignin from kraft black liquors, *Water Res.* 38 (2004) 3043–3050.

[48] X. Wu, L.R. Radovic, Inhibition of catalytic oxidation of carbon/carbon composites by phosphorus, *Carbon* 44 (2006) 141–151.

[49] J. Bedia, J.M. Rosas, D. Vera, J. Rodríguez-Mirasol, T. Cordero, Isopropanol decomposition on carbon based acid and basic catalysts, *Catal. Today* 158 (2010) 89–96.

[50] R. Ruiz-Rosas, J.M. Rosas, I.G. Loscertales, J. Rodríguez-Mirasol, T. Cordero, Electrospinning of silica sub-microtubes mats with platinum nanoparticles for NO catalytic reduction, *Appl. Catal. B Environ.* 156–157 (2014) 15–24.

[51] Z. Liu, Q. Shi, F. Peng, H. Wang, R. Zhang, H. Yu, Pt supported on phosphorus-doped carbon nanotube as an anode catalyst for direct methanol fuel cells, *Electrochim. Commun.* 16 (2012) 73–76.

[52] J.M. Rosas, J. Bedia, J. Rodríguez-Mirasol, T. Cordero, Preparation of hemp-derived activated carbon monoliths. Adsorption of water vapor, *Ind. Eng. Chem. Res.* 47 (2008) 1288–1296.

[53] M.J. Bleda-Martínez, Maciá-Agülló F.J.A. Lozano-Castelló F.D, E. Morallón, D. Cazorla-Amorós, A. Linares-Solano, Role of surface chemistry on electric double layer capacitance of carbon materials, *Carbon* 43 (2005) 2677–2684.

[54] R. Berenguer, H. Nishihara, H. Itoi, T. Ishii, E. Morallón, D. Cazorla-Amorós, et al., Electrochemical generation of oxygen-containing groups in an ordered microporous zeolite-templated carbon, *Carbon* 54 (2013) 94–104.

[55] Y. Shao, G. Yin, Y. Gao, Understanding and approaches for the durability issues of Pt-based catalysts for PEM fuel cell, *J. Power Sources* 171 (2007) 558–566.

[56] C. Huang, T. Sun, D. Hulicova-Jurcakova, Wide electrochemical window of supercapacitors from coffee bean-derived phosphorus-rich carbons, *ChemSusChem* 6 (2013) 2330–2339.

[57] X. Zhao, M. Yin, L. Ma, L. Liang, C. Liu, J. Liao, et al., Recent advances in catalysts for direct methanol fuel cells, *Energy Environ. Sci.* 4 (2011) 2736.

[58] S.P.S. Badwal, S. Giddey, A. Kulkarni, J. Goel, S. Basu, Direct ethanol fuel cells for transport and stationary applications – a comprehensive review, *Appl. Energy* 145 (2015) 80–103.

[59] T. Iwasita, Methanol and CO electrooxidation (Ch. 41), in: W. Vielstich, A. Lamm, H.A. Gasteiger (Eds.), *Handb. Fuel Cells Fundam. Technol. Appl. Electrocatal.*, vol. 2, John Wiley & Sons Ltd., 2003.

[60] D.Y. Chung, K.J. Lee, Y.E. Sung, Methanol electro-oxidation on the Pt surface: revisiting the cyclic voltammetry interpretation, *J. Phys. Chem. C* 120 (2016) 9028–9035.

[61] Z. Liu, X.Y. Ling, X. Su, J.Y. Lee, Carbon-supported Pt and PtRu nanoparticles as catalysts for a direct methanol fuel cell, *J. Phys. Chem. B* 108 (2004) 8234–8240.

[62] M. Ohanian, C.F. Zinola, The anode efficiency in methanol direct fuel cells – a chronoamperometric approach, *J. Power Sources* 168 (2007) 307–322.

[63] B. Braunschweig, D. Hibbitts, M. Neurock, A. Wieckowski, Electrocatalysis: a direct alcohol fuel cell and surface science perspective, *Catal. Today* 202 (2013) 197–209.

[64] H. Liu, C. Song, L. Zhang, J. Zhang, H. Wang, D.P. Wilkinson, A review of anode catalysis in the direct methanol fuel cell, *J. Power Sources* 155 (2006) 95–110.

[65] W.H. Lizcano-Valbuena, V.A. Paganin, E.R. Gonzalez, Methanol electro-oxidation on gas diffusion electrodes prepared with Pt–Ru/C catalysts, *Electrochim. Acta* 47 (2002) 3715–3722.

[66] B. Yang, Q. Lu, Y. Wang, L. Zhuang, J. Lu, P. Liu, et al., Simple and low-cost preparation method for highly dispersed PtRu/C catalysts, *Chem. Mater.* (2003) 3552–3557.

[67] V. Raghubeer, A. Manthiram, Mesoporous carbon with larger pore diameter as an electrocatalyst support for methanol oxidation, *Electrochim. Solid State Lett.* 7 (2004) A336–A339.

[68] S. Domínguez-Domínguez, J. Arias-Pardilla, Á. Berenguer-Murcia, E. Morallón, D. Cazorla-Amorós, Electrochemical deposition of platinum nanoparticles on different carbon supports and conducting polymers, *J. Appl. Electrochem.* 38 (2008) 259–268.

[69] M. Sevilla, C. Salinas Martínez-de Lecea, T. Valdés-Solís, E. Morallón, A.B. Fuertes, Solid-phase synthesis of graphitic carbon nanostructures from iron and cobalt gluconates and their utilization as electrocatalyst supports, *Phys. Chem. Chem. Phys.* 10 (2008) 1433–1442.

[70] S. Beyhan, C. Coutanceau, J.M. Léger, T.W. Napporn, F. Kadırgan, Promising anode candidates for direct ethanol fuel cell: carbon supported PtSn-based trimetallic catalysts prepared by Bönnemann method, *Int. J. Hydrogen Energy* 38 (2013) 6830–6841.

[71] Y. Li, L. Han, B. An, Y. Wang, L. Wang, X. Yin, et al., Preparation of platinum catalysts supported on functionalized graphene and the electrocatalytic properties for ethanol oxidation in direct ethanol fuel cell, *J. Mater. Sci. Mater. Electron.* 27 (2016) 6208–6215.